Using CFD to calculate support interference effect in wind tunnel tests.

Aurélia Cartieri, Patrice Viscat, Sylvain Mouton

USING CFD TO CALCULATE SUPPORT INTERFERENCE EFFECT IN WIND TUNNEL TESTS

Aurélia Cartieri [(1)], Patrice Viscat [(2)], Sylvain Mouton [(3)]

[(1)] ONERA - BP 25 – F-73500 Modane , Email: aurelia.cartieri@onera.fr
[(2)] ONERA – F-92190 Meudon , Email: patrice.viscat@onera.fr
[(2)] ONERA,– F-59045 Lille Cedex, Email: sylvain.mouton@onera.fr

ABSTRACT

This paper adresses the aerodynamic interference effect of two different stings supporting aircraft models during wind tunnel tests. The flow field and forces distortion caused by the sting are assessed by means of steady RANS simulations of the flow. Special attention was paid to the proper derivation of corrections of the incoming flow conditions in terms of Mach number and angle of attack. Comparison against experimental measurements thanks to dummy sting tests in S1MA wind tunnel are provided for validation purpose.

1. INTRODUCTION – STATEMENT OF THE PROBLEM

When simulating an aircraft configuration in a wind tunnel, it is necessary to account – among other corrections – for the support interference effects. Indeed, attaching the model introduces both a change in shape to let the sting enter the model and a flow alteration due to the intrusive support system. This support is shaped to be as small and as discrete as possible, under the constraint that is should sustain forces generated over a wide range of flow conditions and enclose all cables and tubes necessary to supply energy and collect measurements from embarked sensors.
Several recent ([1][3]) or older ([6]) initiatives aimed at determining whether advanced numerical simulations could help in understanding and predicting the support interference effect.
This paper details the methodology adopted to compute sting corrections with RANS CFD and then compares corrections obtained with experimental results.

2. NUMERICAL SIMULATIONS

Solving the steady Reynolds-Averaged Navier-Stokes (RANS) equations for complex configuration has now become routine task in research and industry. It has occasionally been used to model support effects [1][3][5][6] and is regarded as a promising method to supplement classical approaches, either from potential flow theory or from twin sting testing. In this section are described the numerical models and software used to solve the steady RANS equations for the addressed configurations. For all computations, the Mach number and AoA were in the range 0.85 to 0.89 and 0° to 3° for the first model and 0.7 to 0.89 and -3° to 4° for the second one.

2.1. Aircraft model and support

The two aircraft models selected for this study were a full model comprising:

- the fuselage, the wing with four nacelles (non-powered), the vertical and horizontal tail planes (VTP and HTP), named case 1.
- the fuselage, the wing with two nacelles (non-powered), the vertical and horizontal tail planes (VTP and HTP) named case 2.

Both wing shapes are representative of state of the art aerodynamic design for this kind of civil aircraft.
The wind tunnel supports under study in this paper are:

- a straight sting made of cylindrical and conical pieces and penetrating the aircraft fuselage from behind, near the horizontal tail plane;
- a Z-sting, mainly composed of a conical sting supporting a blade which itself penetrates the rear fuselage of the model from below.

These two supports and the models are presented in Fig. 1.

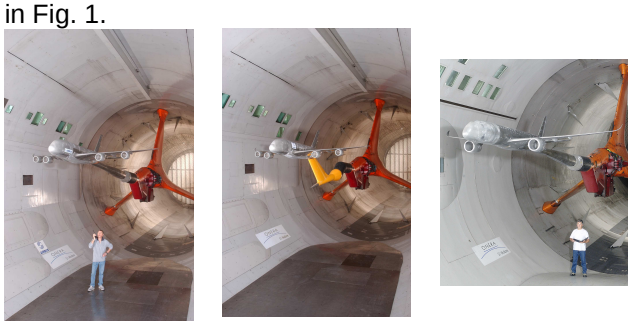

Figure 1 : View of the model and supports

2.2. elsA solver and computations

The *elsA* software is a flow solver developed by Onera and associated partners for aerospace applications [2]. It deals with external and internal aerodynamics. The solver is based on a cell-centered finite volume technique for multiblock structured grids. For this study, the two-equation turbulence model k–ω of Menter was selected.
The boundary layer was modelled on the aircraft and on the support surface thanks to proper boundary conditions and mesh refinement. No reflection boundary condition was used on the far-field surfaces. Mean flow equations were solved thanks to a Jameson second order spatial scheme, using coefficients of artificial dissipation of 0.25 for second order and 0.016 for fourth order, and Martinelli correction with an exponent of 0.3. Iterative method for time marching was a first order backward Euler scheme, associated with implicit scalar LU-SSOR solving with relaxation cycles. To improve convergence, local timestep and a 2-level multigrid cycle were used. The mesh of the configuration takes advantage of the Chimera capabilities of the solver. A mesh of the model itself, comprising about 11 million cells, is realised first. The mesh of the support, comprising about 0.5 million cells, is then built independently and overset with the model mesh as depicted in Fig.2. The individual grids overlap, and once combined cover the entire computational domain. This chimera technique allows computational grids to be generated quickly and easily.

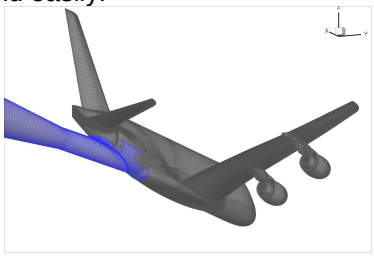

Figure 2 : Surface structured mesh of the case 1 configuration

Provided a suitable mesh of the model is already available, which is generally the case for aircraft under development being tested in wind tunnels, the meshing effort to study support effects is greatly reduced. elsA solver has only been used on the case 1 model.

2.3. TAU solver and computations

The Tau software is a flow solver developed at DLR to simulate the external flows in aerospace applications. A finite volume, cellvertex approach is used on hybrid unstructured grids. This software was only used for comparison purposes.
Computations presented hereafter used the Spallart-Almaras turbulent model. The boundary layer on the model and support is accurately captured thanks to 29 layers of prismatic cells. Proper mesh convergence is ensured thanks to progressive refinement of the grid during the computation. Contrary to elsA computations, one mesh is built for the configuration without support, and another mesh is generated for the configuration with support. The meshes comprised about 12 million points for case 1 and 22 million points for case 2 (see Fig. 3). Mean flow equations were solved thanks to a Jameson second order spatial scheme. Iterative method for time marching was a first order backward Euler scheme, associated with implicit scalar LU-SGS solving with 4 relaxation cycles. To improve convergence, a 3-level multigrid cycle was used.

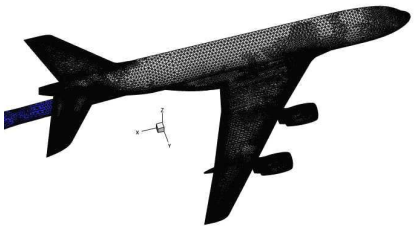

Figure 3 : Surface unstructured mesh of the case 1 configuration.

3. EXPERIMENTAL TESTS

3.1. Facility

S1MA is a continuous atmospheric wind tunnel operating in the sub/transonic regime. It was put into service in 1952 and is equipped with two contrarotating fans, driven by Pelton turbines, the power of which is 88 MW. The wind velocity can be varied from a few meters per second to approximately Mach 1 by varying the fan speed. The total length of the aerodynamic circuit is about 400 m.
A peculiarity of the circuit is the absence of heat exchanger. The temperature is controlled by letting fresh outside air enter the circuit. Hot air naturally exhausts around the edge of the contraction through an annular exit. An exhaust rate of about 10% of the total mass flow is required to maintain a temperature of about 50°C in the tunnel. Among the three interchangeable carts available, cart number 3 has been used for case 1 and cart number 2 for case 2. This test section features solid walls and a geometrical

cross-section of about 45.0 m2. It is well suited to tests on elements of real aircraft and on large scale models.

3.2. Twin sting tests

In order to assess the effect of model supports, dedicated experiments with a dummy sting were realised in S1MA. During these tests, the model is hold in the tunnel thanks to a so-called twin sting rig, which consists in two straight booms, holding the model by the wing lower side (see Fig.4). For these tests, the model's fuselage is cut downstream of the wing. Forces on the rear body are measured thanks to a six-component balance installed in the fuselage whereas forces on the upstream part are not measured.
Measurements are then carried out with and without dummy supports, and the differences interpreted as support effects. The process to compare experiments or computational simulations with and without support will further be developed in section 4. The models were also equipped with static pressure taps.

Figure 4 : Dummy straight sting set up.

3.3. Conventional support corrections

The topic of support correction has been addressed since the advent of wind tunnel testing ([14]) and was dedicated a large amount of studies since then (a sample of which can be found in [9]). A first approach to support interference effects, quite old but still widely used, relies on potential flow theory. It will be shown later that it still can deliver some valuable results at a very cheap cost and is therefore briefly described below. Under the assumption that the flow in the tunnel is irrotational outside the boundary layers and wakes, it can be described by a velocity potential $U_0 x + \varphi$. Assuming now that the velocity perturbations $\partial_x\varphi$, $\partial_y\varphi$ and $\partial_z\varphi$ are small with regard to U_0, one comes to the well-known linearized potential equation:

$$\left(1-M_0^2\right)\partial_x^2\varphi+\partial_y^2\varphi+\partial_z^2\varphi=0\,, \qquad (1)$$

with boundary conditions at solid walls linearized as well.
Unfortunately, this last assumption is less and less valid as the upstream Mach number M_0 approaches 1 and as typical transonic phenomena occurs on the model, with large fluid accelerations up to supersonic regime.
This equation and the corresponding boundary conditions can be solved through a distribution of singularities on the model and support. The intensity of each singularity is based on the cross section areas, the lift and the drag.
Once the proper singularities have been set up, the linearity of equation 1 allows to break down the potential φ into a field φ_m generated by the model and a field φ_s generated by the support. Hence $\nabla\varphi_s = (u_s, v_s, w_s)$ is the field of velocity distortion generated by the support.
Once the velocity field $\nabla\varphi_s$ is known, one can easily determine a field of Mach number distortion:

$$\delta M = M_0\left(1+\frac{\gamma-1}{2}M_0^2\right)\frac{u_s}{U_0}\,, \qquad (2)$$

and a field of angle of attack (AoA) distortion or upwash:

$$\delta\alpha=\frac{w_s}{U_0}\,. \qquad (3)$$

These fields are then averaged in space over areas of aerodynamic significance. This averaging operation lives room for arbitrariness and the following definitions should be regarded merely as conventional, as will be investigated later on.
The Mach number correction ΔM is taken as the value of δM at ¼ of mean aerodynamic chord. The AoA correction is computed from a slightly more elaborated process: it is chord-averaged along the wing span, at ¾ of local chord, this correction enabling the lift correction to be zero (theory of Pistolesi).
A program called DXV877 has been in used in Onera wind tunnels for two decades to perform the above described computations. Results from this software will be referred as "DXV".
This first approach based on potential equation obviously suffers from some shortcomings:

- the range of validity of the linearized potential equation in terms of Mach number is difficult to appreciate;
- results are applicable to correct upstream Mach number and AoA, but not the model forces.

In practice, such an approach must always be complemented by experimental twin sting measurement in order to derive a full set of

support corrections. In order to investigate the limit of validity of the singularity approach, and to provide more complete correction data, more elaborate simulations of the flow field around the model and support were undertaken and are described in the next section.

4. METHOD FOR STING SUPPORT CORRECTION

The first main difficulty arising when considering an aircraft model surrounded by disturbing hardware is to identify a set of equivalent freestream conditions to which one can attribute the measured forces and subsequently make them non dimensional. Like any obstacle, the downstream support generally slows down the flow upstream of itself. Similarly, non-symmetrical devices induce a change in angle of attack on the model. In experiments as in computations, it is therefore necessary to take into account these corrections in Mach number and angle of attack.

4.1. Aerodynamic condition pairing

Let us consider in the Fig. 5 the situation labelled a), which is our reference flow-field without support. The Mach number M_{ref} and AoA α_{ref} of the model can be easily defined by looking at flow conditions far upstream from the model. Pressure and force coefficients are defined in a usual way. Let us now consider the situation labelled b), in which the support was introduced. The upstream Mach number and AoA are now M' and α'. One first effect of the support is to introduce a change ΔM in average Mach number and a change $\Delta\alpha$ in AoA over the model compared to upstream flow condition. For instance, in the present study the support slows the flow down at model location, so that ΔM is negative. This is standard case for support interference [1][3].

Having this in mind, two different approaches can be followed to derive support interference effects [9]:

- let M' be equal to M_{ref} and α' to α, simulate and compare situation b) to a) in order to derive a support effect under the form of force and pressure increments only;
- or let $M'+\Delta M$ be equal to M_{ref} and $\alpha'+\Delta\alpha$ to α_{ref}, then simulate and compare situation b) to a) to derive force and pressure increment. In this case, the support effect is composed of increments of Mach number, AoA, forces and pressure.

In the present study, we adopt the second formulation, arguing that it is close to common wind tunnel definition of the Mach number and AoA which generally includes corrections to cancel mean distortions originating from the support. In fact, ΔM and $\Delta\alpha$ account for mean flow distortion at the model location. If the distortion was homogeneous in space, these corrections would be sufficient to exactly retrieve the reference flow field and forces. Therefore they can be seen as first order correction. The differences in pressure or forces remaining after Mach and AoA corrections account for the inhomogeneity of the distortion generated by the support and can be called second order corrections.

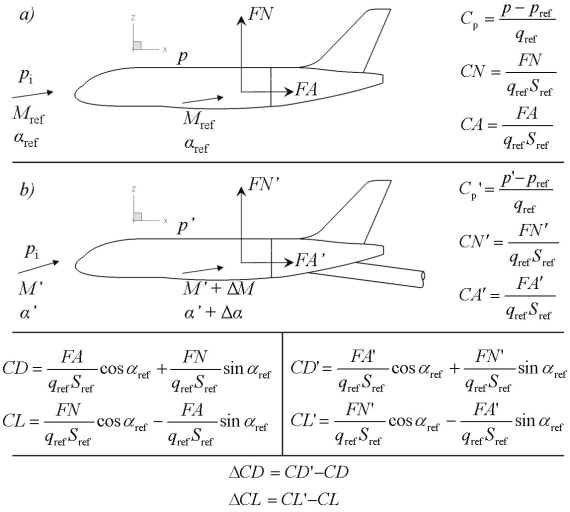

Figure 5 : Nomenclature

One last thing to mention is the use of reference Mach number and AoA to compute force and pressure coefficients, for both situation a) and b).

4.2. Assessment of upstream flow conditions

It was stated in previous section that ΔM and $\Delta\alpha$ account for mean flow distortion at the model location. In order to implement this definition in practical experiments or computations, one needs to address the notion of 'distortion', 'mean' and 'model location'. Once again, any definition implies a part of arbitrariness, justified by physical or practical considerations.

From the standpoint of linearized potential theory, the idea of distortion is straightforward: it is the velocity generated by singularities associated to the support. The averaging process to come up with a mean value was presented in section 3.3.

To deal with numerical simulations, and following [1], let us introduce the following criterion J as the RMS of pressure coefficient distortion on the wing:

$$J = \sqrt{\int_{wing} \left(C_p' - C_p \right)^2 \frac{dS}{S_{wing}}} . \qquad (4)$$

Because Cp' depends on the choice of ΔM and $\Delta\alpha$, J is also a function of ΔM and $\Delta\alpha$. This criterion is expected to be a measurement of the fidelity of the flow with support to the flow without support.
Seeking for a minimum of distortion, let us define:

$$(\Delta M, \Delta\alpha) = \arg\min(J). \qquad (5)$$

With this definition, first order corrections (ΔM, $\Delta\alpha$) are found after a minimization process.

5. VALIDATION AGAINST EXPERIMENTAL TESTS

5.1. Upstream flow corrections

5.1.1. Case 1

In order to identify the corrections defined by Eq. 5, the (ΔM, $\Delta\alpha$) space is sampled until the optimum is identified with sufficient accuracy. From the sampled values, the J-criterion was interpolated by Kriging method to produce the Fig. 6. A qualitative analysis of the obtained database reveals that J is mainly a sensor for the shock wave position, which is mainly driven by the Mach number in the flow condition under study and for this wing design. It explains why the J-criterion is much more sensitive to this variable. Like on most transonic airfoil at design point, the shock wave moves downstream when the Mach number or AoA increases.

a) straight sting b) Z-sting

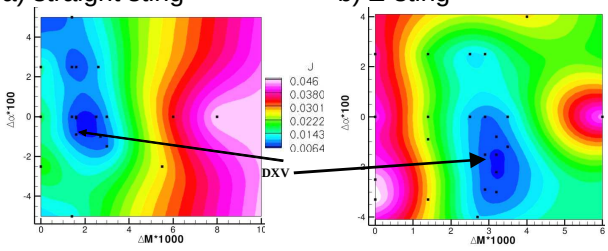

Figure 6 : RMS of wing pressure distribution for various ΔM and $\Delta\alpha$ (TAU computations). Dots indicate sampled points. Reference flow condition is Mach 0.85, AoA 2°.

For the straight sting, the J-criterion leads to an optimum ($\Delta M = -0.0025$, $\Delta\alpha = 0$) against ($\Delta M = -0.0018$, $\Delta\alpha$=0.007) for the ONERA-DXV method.
For the Z sting, The J-criterion leads to an optimum $\Delta M = -0.0032$, $\Delta\alpha = 0{,}015$) against (ΔM=-0.0027, $\Delta\alpha = 0{,}029$) for the ONERA-DXV method.
Having verified that the two models give about the same results, considering the usual order of magnitude of accuracy in wind tunnel (1.10^{-3} in Mach number and 1.10^{-2} in AoA), no systematic research for optimum of J-criterion has carried out with *elsA* computations. The results are now presented with DXV upstream flow corrections.
Even with minimal distortion, a RMS-averaged residual discrepancy of around 0.01 in pressure coefficient remains on the wing, most of which originates from the shock wave area, since the shock position and intensity cannot be exactly reproduced on the whole span when sting is installed, as depicted in Fig. 7.

a) Tau b) elsA

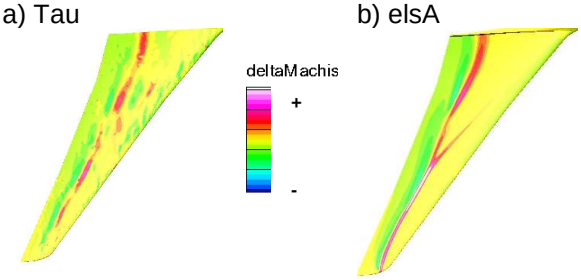

Figure 7 : Distortion of isentropic Mach number on wing due to straight sting at Mach 0.85.

5.1.2. Case 2

For case 2, DXV upstream flow corrections have been used considering what was learned from the case 1.
The residual discrepancy on the isentropic Mach number is depicted in Fig. 8. It is smaller than for case 1.

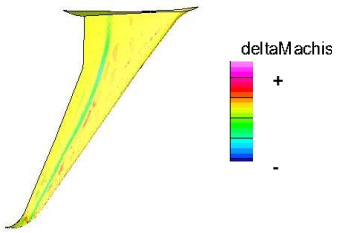

Figure 8 : Distortion of isentropic Mach number on wing due to straight sting with TAU at Mach 0.85.

5.2. Effect on pressure

5.2.1. Straight sting on case 1

Flow distortion generated by the straight sting can be observed in Fig. 9 that displays pressure coefficient distortion on the model skin (obtained by *elsA* and TAU code). Experimental results obtained by twin-sting tests are added to the comparisons. One can observe on the figure that the agreement between CFD and experimental results is rather good. The agreement is less

satisfactory on the rear end of the fuselage, especially with TAU computations which predict a slowdown of the flow on that area, were the boundary layer is closer to separation. This may easily be seen on Fig. 10 which presents pressure distortion on the fuselage at different positions.

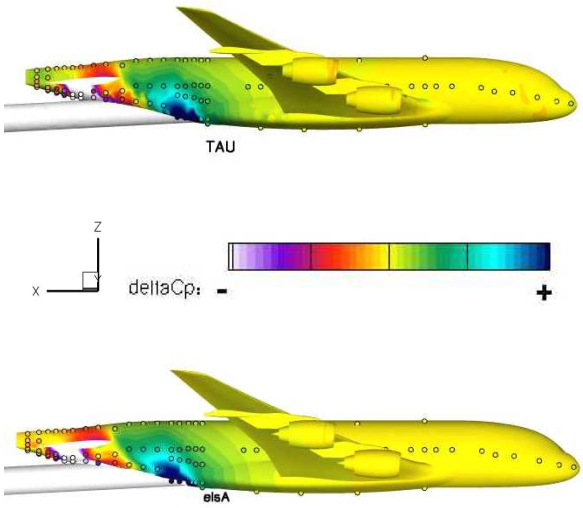

Figure 9 : Distorsion of pressure coefficient on model skin due to straight sting at M_{ref} = 0.85 and α_{ref} = 2°with DXV corrections on Mach and AoA. Circles indicate pressure taps colored by experimental support effect.

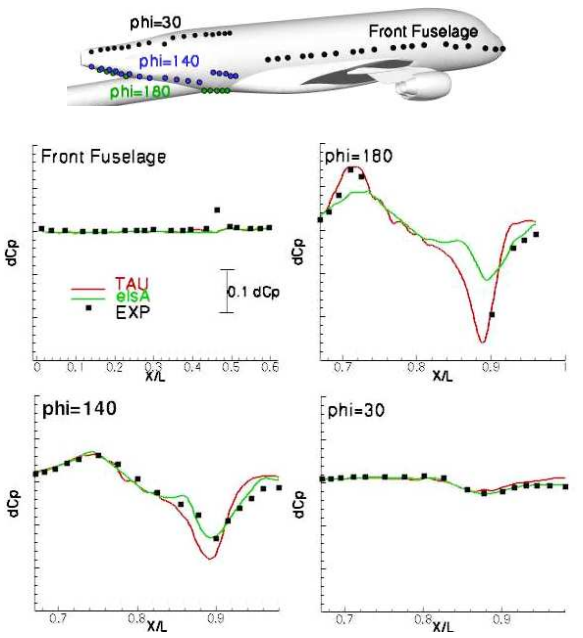

Figure 10 : Pressure increment due to straight sting on the fuselage as computed and measured during twin sting tests.

5.2.2. Z sting on case 1

Flow distortion generated by the Z sting can be observed in Fig. 11 that displays pressure coefficient distortion on the model skin.
Experimental results obtained by twin-sting tests are added to the comparisons. One can observe on the figure that the agreement between CFD and experimental results is good again, even on the rear end of the fuselage where discrepancies existed with straight sting. This can be easily seen on Fig. 12 which presents pressure distortion on the fuselage at different positions.

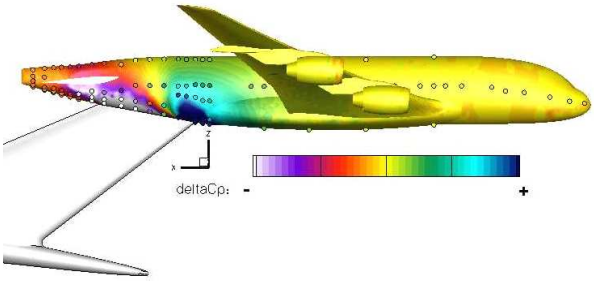

Figure 11 : Distorsion of pressure coefficient on model skin due to Z sting at M_{ref} = 0.85 and α_{ref} = 2°with DXV corrections on Mach and AoA. Circles indicate pressure taps colored by experimental support effect.

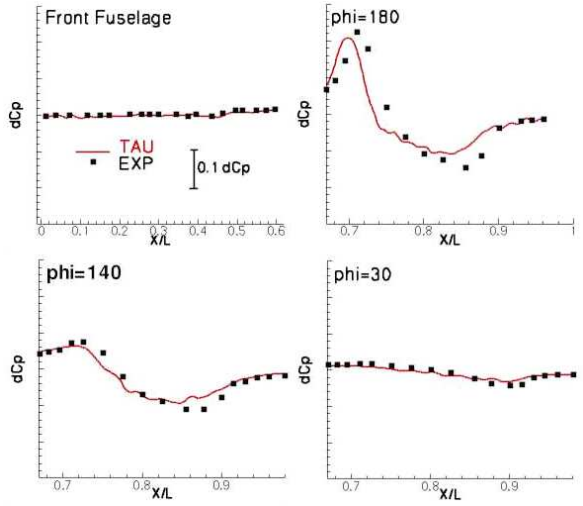

Figure 12 : Pressure increment due to Z sting on the fuselage as computed and measured during twin sting tests.

5.2.3. Straight sting on case 2

No experimental pressure taps are available on the fuselage for that case.
Flow distortion generated by the straight sting can be observed in Fig. 13 that displays pressure coefficient distortion on the model skin.
Pressure coefficient distortion on the HTP at different positions is presented on figure 14. The agreement is good between numerical and experimental results.

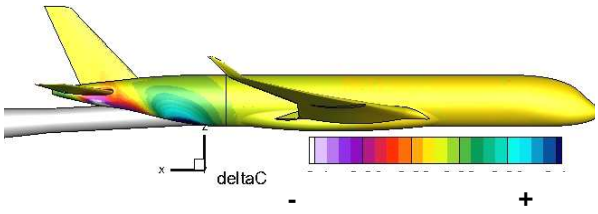

Figure 13 : Distorsion of pressure coefficient on model skin due to straight sting at M_{ref} = 0.85 and α_{ref} = 2° with DXV corrections on Mach and AoA.

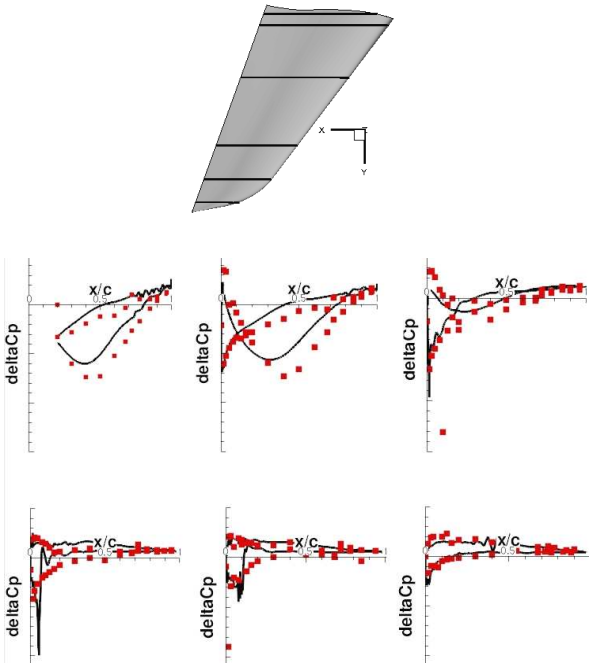

Figure 14 : Pressure increment due to straight sting on the HTP as computed and measured during twin sting tests.

5.3. Effect on forces

5.3.1. Straight sting on case 1

Experimental data available for the rear part (rear body+HTP+VTP) are provided thanks to the balance integrated in the fuselage. The balance reading is corrected (among other phenomena) for split plane pressure.
Comparison of sting effect on forces derived by CFD simulations with the experimental sting effect is carried out in Fig. 15.
Sting effect on drag is different by about 1.5 drag point on the HTP between TAU and elsA computations. Experimental results predict a drag increment of about 3.10^{-4} (cruise lift) on the total rear part whereas TAU and elsA computations predict a drag increment of -2.10^{-4} and 0 respectively. Concerning the front part of the model, no experimental data is available. However there is a good agreement between the calculation by DXV model using the classical Archimedean formula on the one side and the CFD prediction on the other side. The opposite sign of ΔCD for the front and rear body explains why the total experimental drag effect is almost zero.
The effect of supports on lift coefficient is small (less than 0.002) but still has a significant impact on pitching moment due to the lever arm of the rear part. No dependency with AoA is observed in experiment and is accurately predicted by both computations. TAU computations still predict a larger effect than elsA on the HTP.

5.3.2. Z sting on case 1

Comparison of Z-sting effect on forces derived by CFD simulations with the experimental sting effect is carried out in Fig. 16.
Sting effect on drag is very well predicted by computations. The agreement is within $1.5.10^{-4}$ all over the polar range. Here again, good agreement is found between DXV and CFD prediction concerning the drag of the front part.
The effect of supports on lift coefficient is small (less than 0.002). No dependency with AoA is observed in experiment and is accurately predicted by computations.
Concerning pitching moment, the effect is rather large and computations and experimental results are in disagreement. TAU computations predict an effect of 0.007 with no dependency with AoA, Experimental results are constant at 0.002. This shift of 0.005 for the pitching moment coefficient is observed in the simulations with both stings but could not be explained.

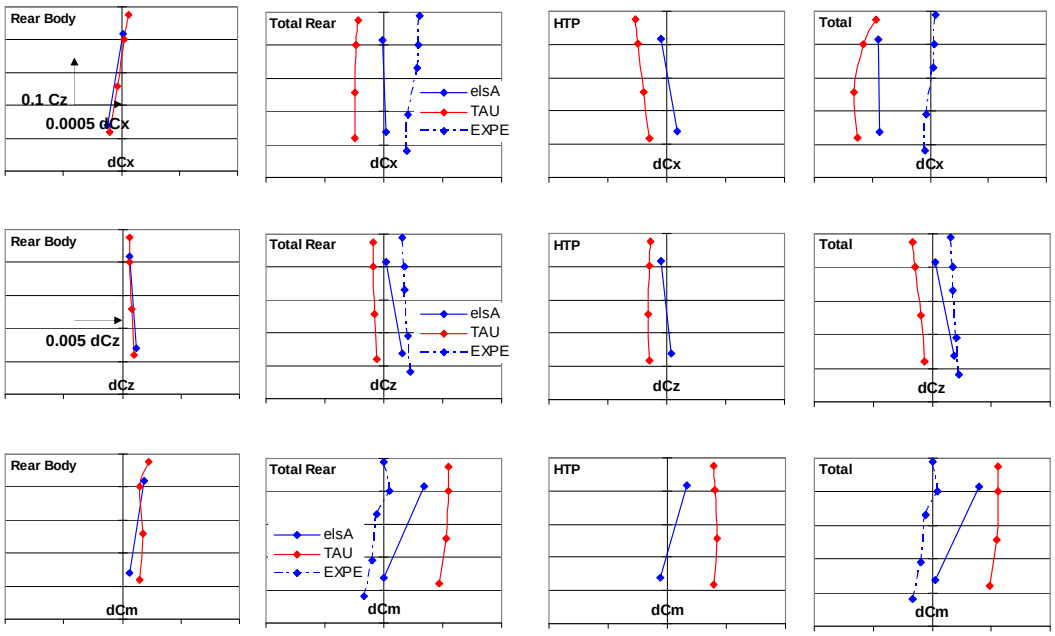

Figure 15 : Force increments due to straight sting on the rear part and on the complete case 1 model as computed by CFD and measured.

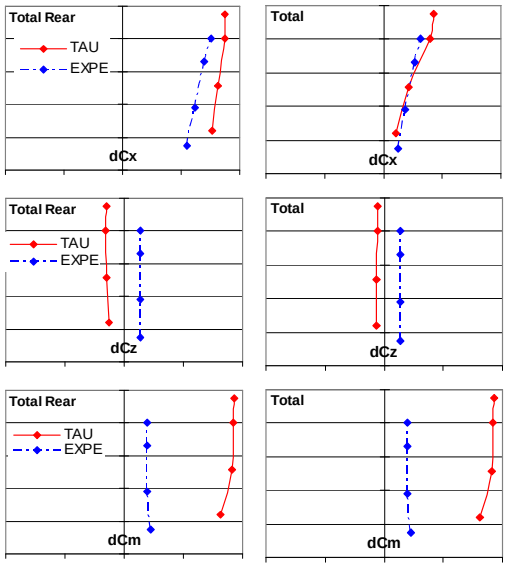

Figure 16 : Force increments due to Z sting on the rear part and on the complete case 1 model as computed by CFD and measured.

5.3.3. Straight sting on case 2

Comparison of straight-sting effect on forces derived by CFD simulations with the experimental sting effect is carried out in Fig. 17.
Sting effect on drag is very well predicted by computations. The agreement is within 1.10^{-4} all over the polar range.
The effect of supports on lift coefficient is extremely small and this is accurately predicted by computations. This is a result of the good prediction of pressure distortion on the HTP observed in section 5.2.3.
As a consequence, the effect on pitching moment is also well predicted by computations.

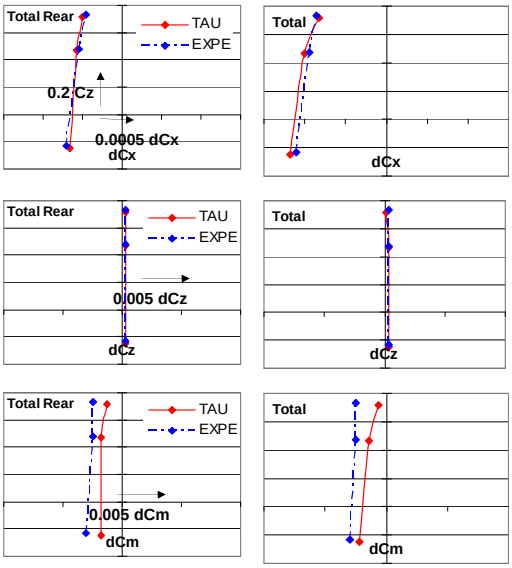

Figure 17 : Force increments due to straight sting on the rear part and on the complete case2 model as computed by CFD and measured.

6. CONCLUSIONS AND PERSPECTIVES

High fidelity CFD method has been applied to the complex case of full industrial wind tunnel models. Special attention was paid to the proper derivation of corrections of the incoming flow conditions in terms of Mach number and angle of attack. The optimised upstream corrections were very close to the DXV calculations. This could allow us to avoid the full exploration of the (ΔM, $\Delta\alpha$) space, which is time consuming. It is also comforting the methods that have been in use for decades to address the sting interference issue.

The simulated sting effects were compared to twin sting tests. Sting effects on lift are small and predicted with only small inaccuracies. However, because of the lever arm, they translate into a constant, unexplained difference of 5.10^{-3} in pitching moment between computations and experiments. This has been observed on case 1 for both stings.

Significant disagreement was observed concerning drag with the straight sting. Investigation are ongoing to check if this might come from the existence of a gap between the sting and the model, which was not modeled. It might be observed however that the total effect on drag is very small, resulting from opposite effects that tend to cancel, which is a situation difficult to properly model. On case 2, drag prediction is much better.

The next step is to assess the cross interaction of wall effect on support interference effect.

7. REFERENCES

1. Mouton S. Numerical Investigations of Model Support Interference in a Transonic Wind Tunnel. *44ème Colloque d'aérodynamique appliqué*e AAAF, Nantes, March 23-25, 2009.
2. Cambier L, Veuillot J-P. *Status of the elsA CFD Software for Flow Simulation and Multidisciplinary Applications.* AIAA 2008-664, Reno, January 7-10, 2008.
3. Mouton S. *Numerical Investigations of Model Support Interference in Subsonic and Transonic Wind Tunnels.* 8th ONERA-DLR Symposium ODAS 2007, Göttingen, October 17-19, 2007

4. Schamborn D, Gerhold T, Heinrich R. The DLR Tau-Code: Recent Applications in Research and Industry. *European Conference on Computational Fluid Dynamics, 2006.*

5. Maina M, Corby N, Crocker EL, Hammond PJ, Wong PWC, *A Feasability Study on Designing Model Support Systems for a Blended Wing Body Configuration in a Transonic Wind Tunnel.* The Aeronautical Journal, January 2006.
6. Bush RH, Jasper DW, Parker SL, Romer WW, Willhite PG. *Computational and Experimental Investigation of F/A-18E Sting Support and Afterbody Distorsion Effects.* Journal of Aircraft, Vol. 33, No. 2, March-April 1996.
7. Lyonnet M, Piat J-F, Roux B, Model Support *Interference Assessment Using a Metric Rear Fuselage and a Twin-Sting at ONERA S2MA Wind Tunnel.* International Conference on Experimental Fluid Mechanics, Turin, July 4-8, 1994.
8. Lynch FT, Crites RC, Spaid FW. *The Crucial Role of Wall Interference, Support Interference, and Flow Field Measurements in the Development of Advanced Aircraft Configurations.* AGARD CP-535, 1993.
9. *Wall Interference, Support Interference and Flow Field Measurements.* AGARD CP-535, 1993.
10. Elsenaar A, Han SOTH, *A Break-Down of Sting Interference Effects.* NLR TP 91220 U, May 1991.
11. Vaucheret X. *Recent Calculation Progress on Wall Interferences in Industrial Wind*

Tunnels. La Recherche Aérospatiale, No. 3, pp 45-47, 1988.

12. Loving DL, Luoma AA. *Sting-Support Interference on Longitudinal Aerodynamic Characteristics of Cargo-Type Airplane Model at Mach 0.70 to 0.84.* NASA Technical Note TN D-4021, July 1967.
13. Love ES. *A Summary of Information on Support Interference Assessment at Transonic and Supersonic Speeds.* NACA RM L53K12, 1954.
14. Pankhurst RC, Holder D. *Wind-Tunnel Technique.* Sir Isaac Pitman & Sons, 1952.